

# The Characteristics of Amorphous-Oxide-Semiconductor Thin-Film-Transistors According to the Active-Layer Structure

Ho-Nyeon Lee<sup>1\*</sup>

<sup>1</sup>Department of Display and Electronic Information Engineering, Soonchunhyang University

## 능동층 구조에 따른 비정질산화물반도체 박막트랜지스터의 특성

이호년<sup>1\*</sup>

<sup>1</sup>순천향대학교 전자정보공학과

**Abstract** Amorphous indium-gallium-zinc-oxide thin-film-transistors (TFTs) were modeled successfully. Dependence of TFT characteristics on structure, thickness, and equilibrium electron-density of the active layer was studied. For mono-active-layer TFTs, a thinner active layer had higher field-effect mobility. Threshold voltage showed the smallest absolute value for the 20 nm active-layer. Subthreshold swing showed almost no dependence on active-layer thickness. For the double-active-layer case, better switching performances were obtained for TFTs with bottom active layers with higher equilibrium electron density. TFTs with thinner active layers had higher mobility. Threshold voltage shifted in the minus direction as a function of the increase in the thickness of the layer with higher equilibrium electron-density. Subthreshold swing showed almost no dependence on active-layer structure. These data will be useful in optimizing the structure, the thickness, and the doping ratio of the active layers of oxide-semiconductor TFTs.

**요 약** 비정질 인듐-갈륨-아연 산화물 박막트랜지스터를 모델링 하여서, 능동층의 구조, 두께, 평형상태의 전자밀도에 대응하는 박막트랜지스터의 특성을 연구하였다. 단일 능동층 박막트랜지스터의 경우, 능동층이 얇을 때 높은 전계효과이동도를 보였다. 문턱전압의 절대값은 능동층의 두께가 20 nm일 때 최저치를 보였으며, 문턱전압이하 기울기는 두께에 대한 의존성을 보이지 않았다. 복층구조 능동층의 경우, 하부의 능동층이 높은 평형상태 전자밀도를 가질 때 보다 우수한 스위칭 특성을 보였다. 이 경우에도 능동층의 두께가 얇을 때 높은 전계효과 이동도를 보였다. 높은 평형상태 전자밀도의 능동층의 두께를 증가시키면 문턱전압은 음의 방향으로 이동하였다. 문턱전압이하 기울기는 능동층의 구조에 대하여 특별한 의존성을 보이지 않았다. 이상과 같은 데이터는 산화물반도체 박막트랜지스터 능동층의 구조, 두께, 도핑비율을 최적화함에 효과적으로 사용될 것으로 기대된다.

**Key Words** : amorphous oxide semiconductor, IGZO, thin-film transistor, active layer, electron density, double layer

## 1. Introduction

The active-matrix flat-panel-display (AMFPD) industry is growing rapidly. Thin-film-transistor liquid-crystal-display (TFT-LCD) is the leading technology for AMFPDs. A new type of AMFPD, the active-matrix organic-light-

emitting-diode (AMOLED), is expected to exceed the success of the TFT-LCD. AMFPD has a circuit in each pixel and by using this pixel circuit, AMFPDs consume less power and have higher picture-quality at a larger size than passive-matrix flat-panel-displays (PMFPDs). Pixel circuits are composed of thin-film transistors (TFTs) and

\*Corresponding Author : Lee, Ho-Nyeon(hnlee@sch.ac.kr)  
Received April 05, 2009      Revised June 15, 2009

Accepted July 22, 2009

capacitors. There have been concerted efforts to make high-quality TFTs because the performance of TFTs is directly related to the display quality of AMFPDs. Up to this point, silicon-based TFTs have mostly been used in the flat panel display (FPD) industry. Amorphous-silicon TFTs (a-Si TFTs) and poly-silicon TFTs (p-Si TFTs) are used for TFT-LCDs and AMOLEDs, respectively. a-Si TFTs can be fabricated using a low-cost process and their performance is good enough for them to be used for TFT-LCDs. However, field-effect mobility and device stability of a-Si TFTs are too poor for them to be used in AMOLEDs because AMOLEDs are current-driven devices that require higher mobility and stability than a TFT-LCD. A p-Si TFT supplies sufficient current and has sufficient stability for application in AMOLEDs. However, the high cost and poor uniformity of p-Si TFTs are obstacles to widespread use of AMOLEDs. Therefore, new AMFPDs such as AMOLEDs require high-performance and low-cost TFTs; however, silicon-based TFTs have limited capability for improved performance.

Recently, oxide semiconductor has begun to be considered as an alternative to silicon semiconductors. The field-effect transistor made of oxide semiconductor was discussed early ago [1]; however, only recently have oxide semiconductors begun to be regarded as a viable alternative to silicon [2,3]. The field-effect mobility of oxide semiconductors has been reported to be about  $1\text{--}80\text{ cm}^2\text{V}^{-1}\text{sec}^{-1}$  [4-6]. These values are sufficient for TFT-LCDs and AMOLEDs; TFT-LCDs and AMOLEDs can be driven using TFTs of about  $1\text{ cm}^2\text{V}^{-1}\text{sec}^{-1}$  mobility and over  $5\text{ cm}^2\text{V}^{-1}\text{sec}^{-1}$  mobility, respectively. An advantage of oxide semiconductors is that the amorphous phase has rather high mobility [7]. Amorphous oxide semiconductors are fabricated using vacuum deposition methods without recrystallization processes such as laser annealing; therefore, uniform characteristics are easily obtained. The mobility of amorphous oxide semiconductors is high enough to drive AMOLEDs. Many transparent conducting oxides including ZnO, SnO, indium zinc oxide (IZO), and indium gallium zinc oxide (IGZO) have been investigated and developed for use in flat-panel electronics. IGZO is considered one of the most promising oxide semiconductors because amorphous IGZO with high mobility has been obtained reproducibly

[7, 8]. Continuous research on oxide-semiconductor thin-film-transistors (OS-TFTs) has resulted in initial characteristics that are superior to those of a-Si; however, their long-term stability is still a problem to be overcome [9, 10]. Recently, oxide semiconductors without indium have attracted attention because indium is becoming more expensive [11, 12]. AMOLED prototypes using OS-TFTs have been developed by a few manufacturers. Performance of the prototypes was good enough for some practical displays [13, 14]. Currently, OS-TFTs are expected to succeed Si-TFTs in the flat-panel display (FPD) industry.

As described above, developing OS-TFT technology is important for the FPD industry. In addition, many transparent electronic devices will require OS-TFT technology; OS-TFT is an essential part of smart windows and transparent displays. These transparent electronics are forecasted to be important commercial electronics in near future. A transparent switching device is one of the main issues in transparent electronics development, and, until now, OS-TFT has been the best candidate for this application.

Considerable OS-TFT research has focused on materials and process. However, device structures have not been well studied. Optimized device structures are required to make practical OS-TFTs. In this work, I have performed optimization studies. The dependence of OS-TFT performance on the structure, the thickness, and the equilibrium charge-carrier concentration (related to the doping ratio) of oxide-semiconductor active-layers was carefully examined. OS-TFTs were modeled using Silvaco's simulation tools with parameters extracted from various previous reports. From this work, useful data on the active-layer structure, thickness, and doping ratio are provided to facilitate optimization of the performance of OS-TFTs.

## 2. Modeling and Parameters

Amorphous IGZO was modeled using a device simulator, ATLAS, from Silvaco [15]. The subgap density of states (DOSs) needs to be specified for TFT characteristics. These comprise band-tail states and deep-level states. Exponential DOSs for band-tail states

and Gaussian DOSs for deep-level states were used as in a-Si TFTs. Acceptor-like band-tail states and donor-like band-tail states can be described as follows:

$$g_{TA} = N_{TA} \exp\left[\frac{E - E_C}{w_{TA}}\right] \quad (1)$$

$$g_{TD} = N_{TD} \exp\left[\frac{E_V - E}{w_{TD}}\right] \quad (2)$$

where  $E$  is the trap energy,  $E_C$  and  $E_V$  are the conduction band edge and the valence band edge, respectively,  $g_{TA}(E)$  and  $g_{TD}(E)$  are the density of states (DOSs) of acceptor-like band-tail states and donor-like band-tail states, respectively,  $N_{TA}$  and  $N_{TD}$  are conduction-band and valence-band edge-intercept-densities, respectively, and  $w_{TA}$  and  $w_{TD}$  are characteristic decay energies of acceptor-like and donor-like band-tail states, respectively. Deep-level states were also classified as acceptor-like and donor-like states. These states can be described as follows:

$$g_{GA}(E) = N_{GA} \exp\left[-\left[\frac{E_{GA} - E}{w_{GA}}\right]^2\right] \quad (3)$$

$$g_{GD}(E) = N_{GD} \exp\left[-\left[\frac{E - E_{GD}}{w_{GD}}\right]^2\right] \quad (4)$$

where  $N_{GA}$  and  $N_{GD}$  are total DOSs of acceptor-like states and donor-like states, respectively,  $w_{GA}$  and  $w_{GD}$  are characteristic decay energies of the acceptor-like states and donor-like states, respectively, and  $E_{GA}$  and  $E_{GD}$  are peak energies of distributions of the acceptor-like states and donor-like states, respectively. From above, the total DOS in the gap can be calculated as follows:

$$g(E) = g_{TA}(E) + g_{TD}(E) + g_{GA}(E) + g_{GD}(E) \quad (5)$$

The parameters used in this work were as follows. The band gap ( $E_C - E_V$ ) was 3.4 eV [16], the electron affinity was 4.29 eV [17], the dielectric constant was 8.12 [18], and the donor level was 0.03 eV [17].  $N_{TA}$ ,  $w_{TA}$ ,  $N_{GA}$ ,  $w_{GA}$ , and  $E_{GA}$  were  $2.3 \times 10^{18} \text{ cm}^{-3} \text{ eV}^{-1}$ , 0.08 eV,  $3.2 \times 10^{16}$

$\text{cm}^{-3}$ , 1.5 eV, and 3.4 eV, respectively [19]. Effective densities of state function in the conduction band ( $N_C$ ) and the valence band ( $N_V$ ) were estimated using the following equations:

$$N_C = 2 \left( \frac{2\pi m_n^* k T}{h^2} \right)^{3/2} \quad (6)$$

$$N_V = 2 \left( \frac{2\pi m_p^* k T}{h^2} \right)^{3/2} \quad (7)$$

The effective mass of electrons ( $m_n^*$ ) in the conduction band and the effective mass of holes ( $m_p^*$ ) in the valence band were  $0.318 m_0$  [18] and  $0.5 m_0$  [20], respectively, where  $m_0$  is electron mass.  $T$ ,  $k$ , and  $h$  refer to absolute temperature, Boltzmann's constant, and Planck's constant, respectively. The temperature was fixed at 300 K. Using these parameters and Eqs. (6) and (7),  $N_C$  and  $N_V$  were calculated as  $4.5 \times 10^{18} \text{ cm}^{-3}$  and  $8.87 \times 10^{18} \text{ cm}^{-3}$ , respectively. Bulk electron mobility ( $\mu_n$ ) was  $15 \text{ cm}^2 \text{ V}^{-1} \text{ sec}^{-1}$ , chosen to meet the general range of reports [7, 21, 22]. Donor-like states in the gap were neglected because oxide semiconductors considered in this work were n-type; donor-like states in the gap barely influenced the characteristics of TFTs made of n-type active layers as in this work.

Fig. 1 shows the basic structure of TFTs used in this work. A bottom-gate/top-contact structure was used. Channel width and length were  $500 \mu\text{m}$  and  $100 \mu\text{m}$ , respectively. Gate, source, and drain electrodes were made from aluminum. The work function of aluminum was 4.6 eV. Amorphous silicon nitride was used for the gate insulator and the passivation. The thickness of the gate insulator and the passivation were 300 nm and 200 nm, respectively.

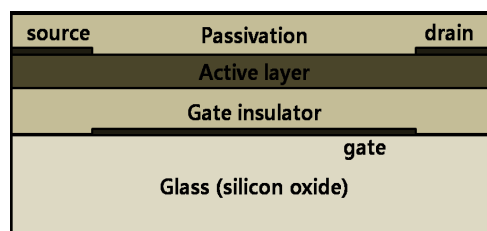
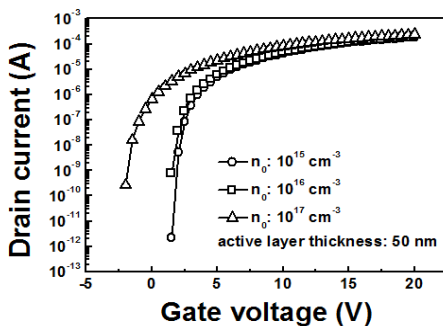


[Fig. 1] The TFT structure used for this work.

Field-effect mobility ( $\mu_{FE}$ ) and threshold voltage ( $V_{TH}$ ) were obtained from the slope and the intercept of the curve of square root of drain current ( $I_D$ ) in saturation region, respectively. Subthreshold swing (SS) was obtained from the  $I_D$  curve as a function of gate bias voltage ( $V_G$ ) using the equation of  $dV_G/d\log_{10}(I_D)$ .

### 3. Mono Active Layer

Fig. 2 shows the drain current ( $I_D$ ) characteristics as a function of gate bias voltage ( $V_G$ ). The active layer was a 50 nm oxide-semiconductor layer. As shown in Fig. 2,  $I_D$ - $V_G$  curves were built well using the simulation model described in the previous section. Transfer curves depended on equilibrium electron-density ( $n_0$ ). As shown in the figure, a TFT with  $10^{17} \text{ cm}^{-3} n_0$  had a relatively large current at zero gate-bias.



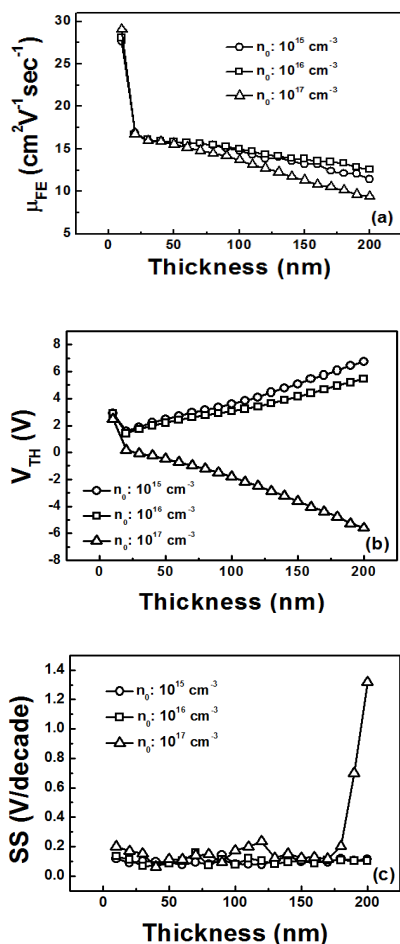
[Fig. 2] Drain currents of TFTs with mono active layers as a function of gate bias voltage. The active layer thickness was 50 nm. Drain-source voltage was 10 V.

Fig. 3(a) shows  $\mu_{FE}$  according to the thickness of the active layer.  $\mu_{FE}$ s of TFTs with  $n_0$  of  $10^{15} \text{ cm}^{-3}$  and with  $n_0$  of  $10^{16} \text{ cm}^{-3}$  were similar to each other. However, a TFT with  $10^{17} \text{ cm}^{-3} n_0$  gave much less  $\mu_{FE}$ .  $\mu_{FE}$  gradually decreased after a sharp initial drop as a function of increasing active layer thickness. As shown in the figure, the TFT with the thinner active layer showed higher field-effect mobility. The TFT with the 10 nm active layer showed the highest  $\mu_{FE}$ . Especially for TFTs with high  $n_0$ , a thin active layer should be used to obtain high  $\mu_{FE}$ . Charge-density modulation of the upper side of the active layer became difficult as the active-layer

thickness increased due to the electric-field shield-effect of accumulated charges on the front side. This effect became severe for the case of high  $n_0$ .

$V_{TH}$  showed the smallest absolute values for the 20 nm active-layers. For  $10^{15} \text{ cm}^{-3} n_0$  and  $10^{16} \text{ cm}^{-3} n_0$ ,  $V_{TH}$  variations as a function of active layer thickness were less than the  $10^{17} \text{ cm}^{-3} n_0$  case. As shown in Fig. 3(b),  $V_{TH}$ s decreased noticeably when the active layer thickness increased from 10 nm to 20 nm. After this,  $V_{TH}$ s increased in the positive direction as the active layer thickness increased. In the cases of these low carrier density active layers, the voltage drop at the source side between the top surface and the bottom surface of the active layer can be increased significantly due to the rather high resistivity of the active layer as the thickness of active layer increases. Therefore, larger positive voltage is needed to turn on TFTs having thicker active layer. For the  $10^{17} \text{ cm}^{-3} n_0$  case,  $V_{TH}$  increased steeply to negative values with increasing active-layer thickness. This occurred because there were many electrons in the active layer with  $10^{17} \text{ cm}^{-3} n_0$ ; a larger negative voltage needs to be applied to the gate to deplete the channel as active-layer thickness increases. That is,  $V_{TH}$  will become more negative as the thickness of the active layer increases.

The variation in SS is reported in Fig. 3(c). TFTs with  $n_0$  of  $10^{15} \text{ cm}^{-3}$  and  $10^{16} \text{ cm}^{-3}$  showed subthreshold swings that were nearly independent of the active-layer thickness and  $n_0$ . For the case of  $10^{17} \text{ cm}^{-3} n_0$ , subthreshold behavior could be divided into two regions. For the thinner-active-layer region under 170 nm, subthreshold behavior was similar to those of  $10^{15} \text{ cm}^{-3} n_0$  and  $10^{16} \text{ cm}^{-3} n_0$ . For the thicker-active-layer region over 170 nm, SS showed higher values as the active layer thickness increased. This increase seemed to be related to electric-field shielding. When active-layer thickness was under 170 nm, SS was nearly independent of the active-layer thickness and  $n_0$ .



[Fig. 3] Characteristics of TFTs with mono active layers as a function of the active layer thickness; (a) field-effect mobility ( $\mu_{FE}$ ), (b) threshold voltage ( $V_{TH}$ ), and (c) subthreshold swing (SS). Drain-source voltage was 10 V.

#### 4. Double Active Layer

Fig. 4 shows  $I_D$ - $V_G$  curves of TFTs with double active layers. The TFT structure was the same as that of the TFT with a mono active layer except for the active layer. In this section, the active layer was composed of two layers with different  $n_0$ . Fig. 4(a) shows results of TFTs with 50 nm thick active layers. The bottom-active-layer  $n_0$  and top-active-layer  $n_0$  were  $10^{17} \text{ cm}^{-3}$  and  $10^{15} \text{ cm}^{-3}$ , respectively. The turn-on voltage showed a noticeable difference; however, on-current hardly changed between

TFTs with different bottom-active-layer thicknesses. Fig. 4(b) is the result of TFTs with 100 nm active layers;  $n_0$  of the bottom active layer was  $10^{17} \text{ cm}^{-3}$  and of the top active layer was  $10^{15} \text{ cm}^{-3}$ . Switching performances became worse with thicker bottom active layers; performance variation was larger than that of TFTs with 50 nm active layers. On-current increased slightly as the bottom active layer thickness increased. Fig. 4(c) gives results for TFTs with 50 nm thick active layers. The bottom active layer had  $10^{15} \text{ cm}^{-3}$   $n_0$  and the top active layer had  $10^{17} \text{ cm}^{-3}$   $n_0$ . The turn-on voltage showed a noticeable difference and the on-current decreased slightly as the bottom active layer thickness increased. Fig. 4(d) shows results of TFTs with 100 nm thick active layers; the  $n_0$  of the bottom active layer was  $10^{15} \text{ cm}^{-3}$   $n_0$  and the  $n_0$  of the top active layer was  $10^{17} \text{ cm}^{-3}$ . TFTs with thicker bottom active layers gave better switching performance though their performance variation was greater than that of TFTs with 50 nm active layers. There was a noticeable decrease in on-current with increasing bottom-active-layer thickness. A comparison between TFTs with a higher  $n_0$  bottom active layer and lower  $n_0$  bottom active layer is shown in Fig. 5. On-currents were almost the same; however, the switching performance of a TFT with a higher  $n_0$  bottom active layer was better.

Fig. 6(a) shows  $\mu_{FE}$  of various TFTs. TFTs with bottom active layers of  $10^{17} \text{ cm}^{-3}$   $n_0$  had better mobility in the low to medium thickness range of the bottom active layer.  $\mu_{FE}$  of TFTs with bottom active layers of  $10^{15} \text{ cm}^{-3}$   $n_0$  increased gradually according to the increase in bottom-active-layer thickness and then showed higher values for a thicker bottom active-layer. For the TFTs having 100 nm active layers, increase of  $\mu_{FE}$  according to the increase of bottom layer thickness was significant for the case of bottom active layers of  $10^{17} \text{ cm}^{-3}$   $n_0$ . This can be understood considering the results of mono-active layer; the lower  $n_0$  active layer gave the higher  $\mu_{FE}$ . TFTs with bottom active layers of  $10^{15} \text{ cm}^{-3}$   $n_0$ ; thinner bottom means larger portion of top layer with  $10^{17} \text{ cm}^{-3}$   $n_0$  causing lower  $\mu_{FE}$ . Therefore, thicker bottom layer with  $10^{15} \text{ cm}^{-3}$   $n_0$  makes layer  $\mu_{FE}$ . For both cases of bottom active layer  $n_0$ s, mobility increased when the total thickness of the active layer was lower due to ease of modulating the charge density of the thinner active layer.

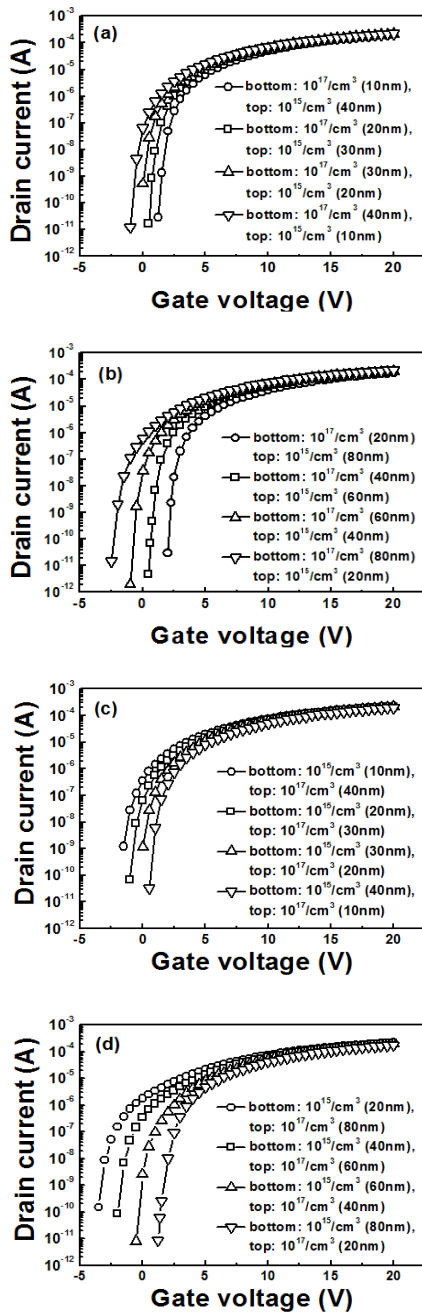


[Fig. 4] Drain currents of TFTs with double active layers as a function of gate bias voltage. Drain-source voltage was 10 V.

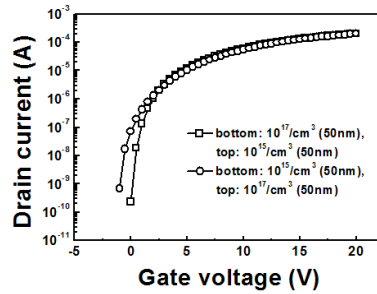


[Fig. 5] Drain currents of TFTs with double active layers as a function of gate bias voltage; the layers with  $10^{17} \text{ cm}^{-3} n_0$  and  $10^{15} \text{ cm}^{-3} n_0$  had the same thickness (50 nm). The total thickness of the active layer was 100 nm. Drain-source voltage was 10 V.

Threshold voltage variations are shown in Fig. 6(b). For TFTs with bottom active layers of  $10^{17} \text{ cm}^{-3} n_0$ ,  $V_{\text{THS}}$  decreased as bottom-active-layer thickness increased. For TFTs with bottom active layers of  $10^{15} \text{ cm}^{-3} n_0$ ,  $V_{\text{THS}}$  increased as the bottom active layer thickness increased. TFTs with bottom active layers of  $10^{17} \text{ cm}^{-3} n_0$  with 50 nm active layers and with 100 nm active layers gave  $V_{\text{THS}}$  near 0 V for bottom active layer thicknesses of 40 nm and 70 nm, respectively. TFTs with bottom active layers of  $10^{15} \text{ cm}^{-3} n_0$  with 50 nm active layers and with 100 nm active layers gave  $V_{\text{THS}}$  near 0 V for bottom active layer thicknesses of 10 nm and 30 nm, respectively. As shown in the figure,  $V_{\text{TH}}$  could be controlled by adjusting the thickness of the layer with  $10^{17} \text{ cm}^{-3} n_0$ . As the thickness of the high  $n_0$  layer increased, more electrons appeared in the conduction channel even with an unbiased gate. Therefore,  $V_{\text{TH}}$  shifted negatively as a function of the increase in the thickness of the layer with  $10^{17} \text{ cm}^{-3} n_0$ .

Fig. 6(c) shows subthreshold swings of TFTs with double active layers. SS showed little dependency on the bottom-active-layer thickness and  $n_0$ . TFTs with the bottom active layer of  $10^{15} \text{ cm}^{-3} n_0$  and a total active-layer thickness of 100 nm showed more variation; however, all SS values in this figure were low enough for the TFTs to be used for FPDs.

In the case of the double active layer, better switching performances were obtained for TFTs with bottom active layers with  $10^{17} \text{ cm}^{-3} n_0$ . This was because the bottom active layer with higher  $n_0$  caused higher electron density in the current path at the front channel; this produced a

higher on-current, and a top active layer with lower  $n_0$  was easier to deplete for the off state.

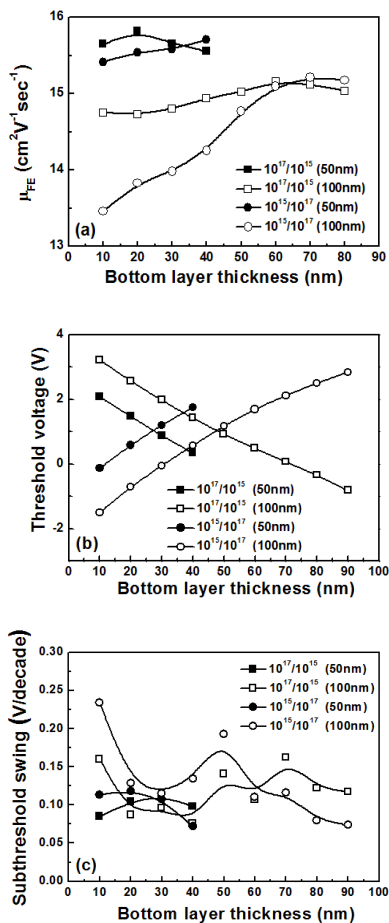


[Fig. 6] Characteristics of TFTs with double active layers as a function of the active layer thickness; (a) field-effect mobility ( $\mu_{FE}$ ), (b) threshold voltage ( $V_{TH}$ ), and (c) subthreshold swing (SS). Drain-source voltage was 10 V.

## 4. Conclusions

Modeling was successful in producing transfer curves of OS-TFTs. Dependencies of TFT characteristics on active layer structure, active layer thickness, and equilibrium electron density were estimated. For mono-active-layer TFTs, thinner active layers produced higher field-effect mobility.  $V_{TH}$  showed the smallest value for the 20 nm active-layer. Subthreshold swing

showed almost no dependence on active-layer thickness. For the double-active-layer case, better switching performances were obtained for TFTs with bottom active layers with higher equilibrium electron-density. TFTs with thinner active layers had higher mobility.  $V_{TH}$  shifted negatively with increasing layer thickness with higher equilibrium electron-density. Subthreshold swing showed almost no dependence on active-layer structure. These data will be beneficial for optimizing the structure, the thickness, and the doping ratio of the active layer of oxide-semiconductor TFTs.

## References

- [1] G. F. Bosen and J. J. Jacobs, "ZnO Field-Effect Transistor", Proc. IEEE, pp. 2094-2095, 1968.
- [2] T. Hirao, M. Furuta, H. Furuta, T. Matsuda, T. Hiramatsu, H. Hokari, M. Yoshida, H. Ishii and M. Kakegawa, "Novel top-gate zinc oxide thin-film transistors (ZnO TFTs) for AMLCDs", J. Soc. Information Display, vol. 15, pp. 17-22, 2007.
- [3] P. Carcia, R. McLean and M. Reilly, "Oxide engineering of ZnO thin-film transistors for flexible electronics", J. Soc. for Information Display, vol. 13, pp. 547-554, 2005.
- [4] N. L. Dehuff, E. S. Kettenring, D. Hong, H. Q. Chang and J. J. Wager, "Transparent thin-film transistors with zinc indium oxide channel laer", Journal of Applied Physics. vol. 97, pp. 064505, 2005.
- [5] W. B. Jackson, G. S. Herman, R. L. Hoffmann, C. Taussig, S. Braymen, F. Jeffery and J. Hauschildt, "Zinc tin oxide transistors on flexible substrates", J. Non-Cryst. Solids, vol. 352, pp. 1753-1755, 2006.
- [6] K. Nomura, H. Ohta, K. Ueda, T. Kamiya, M. Hirano and H. Hosono, "All oxide transparent MISFET using high-k dielectrics gates", Microelectronic Engineering, vol. 72, pp. 294-298, 2004.
- [7] K. Nomura, H. Ohta, A. Takagi, T. Kamiya, M. Hirano and H. Hosono, "Room-temperature fabrication of transparent flexible thin-film transistors using amorphous oxide semiconductors", Nature, vol. 432, pp. 488-492, 2004.
- [8] H. Hosono, "Ionic amorphous oxide semiconductors: Material design, carrier transport, and device application", J. Non-Cryst. Solids, vol. 352, pp. 851-858, 2006.

- [9] J. K. Jeong, H. W. Yang, J. H. Jeong, Y. G. Mo and H. D. Kim, "Origin of threshold voltage instability in indium-gallium-zinc oxide thin film transistors", *Appl. Phys. Lett.*, vol. 93, pp. 123508, 2008.
- [10] J. M. Lee, I. T. Cho, J. H. Lee and H. I. Kwon, "Bias-stress-induced stretched-exponential time dependence of threshold voltage shift in InGaZnO thin film transistors", *Appl. Phys. Lett.*, vol. 93, pp. 093504, 2008.
- [11] I. Titkov, I. Pronin, I. Liniichuk and I. Grekhov, "Transparent ferroelectric field effect transistors with a single-crystal SnO<sub>2</sub> channel", *Integr. Ferroelectr.* vol. 72, pp. 53-60, 2005.
- [12] D. Cho, Sh. Yang, C. Byun, J. Shin, M. Ryu, S. Park, C. Hwang, S. Chung, W. Cheong, S. Yoon and H. Chu, "Transparent Al - Zn - Sn - O thin film transistors prepared at low temperature", *Appl. Phys. Lett.*, vol. 93, pp. 142111, 2008.
- [13] H. D. Kim, J. K. Jeong, Y. G. Mo and H. K. Chung, "Oxide TFT as an Emerging Technology for Next Generation Display", *Proc. Int. Meeting on Information Display*, pp. 119-122, 2008.
- [14] J. H. Lee, D. H. Kim, D. J. Yang, S. Y. Hong, K. S. Yoon, P. S. Hong, C. O. Jeong, H. S. Park, S. Y. Kim, S. K. Lim, S. S. Kim, K. S. Son, T. S. Kim, J. Y. Kwon and S. Y. Lee, "World's Largest (15-inch) XGA AMLCD Panel Using IGZO Oxide TFT", *Soc. Information Display 2008 Int. Symp. Digest of Tech. Papers*, pp. 625-628, 2008.
- [15] ATLAS User's Manual (Silvaco International, Santa Clara, California, 2007).
- [16] A. Ohtomo, K. Tamura, K. Saikusa, K. Takahashi, T. Makino, Y. Segawa, H. Koinuma and M. Kawasaki, "Single crystalline ZnO films grown on lattice-matched ScAlMgO<sub>4</sub>(0001) substrates", *Appl. Phys. Lett.*, vol. 75, pp. 2635-2637, 1999.
- [17] K. B. Sundaram and A. Khan, "Work function determination of zinc oxide films", *J. Vac. Sci. Technol. A*, vol. 15, pp. 428-430, 1997.
- [18] Rode, D. L., *Semiconductors and Semimetals*, R. K. Willardson and A. C. Beer, eds., Academic Press, N.Y., vol. 10, p. 1, 1975.
- [19] H. H. Hsieh, T. Kamiya, K. Nomura, H. Hosono and C. C. Wu, "Modeling of amorphous InGaZnO<sub>4</sub> thin film transistors and their subgap density of states", *Appl. Phys. Lett.*, vol. 92, pp. 133503, 2008.
- [20] L. Bornstein, in *Semiconductors*, edited by O. Medelung (Springer, Berlin, 1998), vol III-17, pp. 35-115.
- [21] P. Barquinha, A. Pimentel, A. Marques, L. Pereira, R. Martins, E. Fortunato, "Effect of UV and visible light radiation on the electrical performances of transparent TFTs based on amorphous indium zinc oxide", *J. Non-Cryst. Solids*, vol. 352, pp. 1756- 1760, 2006.
- [22] M. S. Grover, P. A. Hersh, H. Q. Chiang, E. S. Kettenring, J. F. Wager and D. A. Keszler, "Thin-film transistors with transparent amorphous zinc indium tin oxide channel layer", *J. Phys. D: Appl. Phys.*, vol. 40, pp. 1335-1338, 2007.

---

### Ho-Nyeon Lee

[Regular member]



- Aug. 1997 : Korea Advanced Instituted of Science and Technology, PhD in Physics.
- Aug. 1997 ~ Jun. 2001 : HYNIX, Research Engineer
- Jul. 2001 ~ Mar. 2004 : HYDIS Technology, Research Engineer
- Apr. 2004 ~ Aug. 2006 : Samsung Advanced Institute of Technology, Research Scientist
- Sep. 2006 ~ current : Soonchunhyang Univ., Dept. of Display & Electronic Information Engineering, Professor

<Research Interests>

Information Display, Solar Energy